Advances in Applied Mathematics and Mechanics
Adv. Appl. Math. Mech., Vol. **2**, No. 2, pp. 131-159

DOI: 10.4208/aamm.09-m0971
April 2010

A Numerical Study of Two-Fluid Models with Pressure and Velocity Relaxation

Svend Tollak Munkejord[1,*]

[1] *SINTEF Energy Research, Sem Sælands veg 11, NO-7465 Trondheim, Norway*

Received 22 July 2009; Accepted (in revised version) 16 November 2009

Available online 5 March 2010

Abstract. This paper presents a study of pressure and velocity relaxation in two-phase flow calculations. Several of the present observations have been made elsewhere, and the purpose of the paper is to strengthen these observations and draw some conclusions. It is numerically demonstrated how a single-pressure two-fluid model is recovered when applying instantaneous pressure relaxation to a two-pressure two-fluid model. Further, instantaneous velocity relaxation yields a drift-flux model. It is also shown that the pressure relaxation has the disadvantage of inducing a large amount of numerical smearing. The comparisons have been conducted by using analogous numerical schemes, and a multi-stage centred (MUSTA) scheme for non-conservative two-fluid models has been applied to and tested on the two-pressure two-fluid model. As for other, previously tested two-phase flow models, the MUSTA schemes have been found to be robust, accurate and non-oscillatory. However, compared to their Roe reference schemes, they consistently have a lower computational efficiency for problems involving mass transport.

AMS subject classifications: 76T10, 76M12, 65M12, 35L65.

Key words: Two-phase flow, two-fluid model, MUSTA scheme, pressure relaxation, velocity relaxation.

1 Introduction

The modelling of dynamic two-phase flows has a large range of industrial applications, including the transport of oil and gas, energy processes, and safety analyses of nuclear power plants. This kind of modelling is challenging in several ways. First, the Navier–Stokes equations are averaged, see [12]. This brings forward unknown terms for which it is necessary to find models. Unfortunately, the "basic" two-fluid model, in which as many closure terms as possible have been set to equal to zero, has

*Corresponding author.
URL: `http://www.pvv.org/~stm/research/`
Email: stm@pvv.org (S. T. Munkejord)

complex eigenvalues [33]. Further, in its hyperbolic region, the two-fluid model has several waves whose velocity may vary greatly. This, as well as the appearance of non-conservative terms, makes it challenging to construct robust and accurate numerical methods [5, 32, 45].

The two-pressure two-fluid model has an eigenstructure which lends itself much more easily to analysis than that of the "basic" single-pressure two-fluid model. Furthermore, the two-pressure two-fluid model is hyperbolic everywhere, except at the sonic points [35]. However, for a large class of two-phase flow problems of interest, the phasic pressures are so strongly coupled that a pressure-relaxation procedure is required.

Saurel and Abgrall [36] discussed a two-fluid model augmented by a volume-fraction advection equation and so yielding a two-pressure model. It can be thought of as an extension of the Baer and Nunziato [3] model. The two-pressures-with-instantaneous-pressure-relaxation method has been investigated by several researchers [2, 20, 22, 24]. Still, however, there is a need to clarify the potential advantages of this approach, as opposed to using a more "direct" flow model and then solving it using a suitable numerical method for non-conservative balance laws.

The multi-stage centred (MUSTA) scheme [39,41,42] is aimed at coming close to the accuracy of upwind schemes while retaining the simplicity of centred schemes. It does not require any information of the eigenstructure of the model, except for an estimate of the maximum eigenvalue for the Courant-Friedrichs-Lewy (CFL) criterion. Instead, the Riemann problem at the cell interface is approximated numerically by employing a first-order centred scheme on a local grid. The MUSTA scheme has been tested on the Euler equations [39, 44], as well as on a drift-flux two-phase flow model [27] and on the shallow-water equations [17]. Munkejord et al. [28] derived a MUSTA scheme for the two-fluid model with or without an energy equation by using the framework of formally path-consistent schemes of Castro et al. [32] and Parés [6].

The contribution of this paper is to clarify and strengthen previous observations by several authors, that in some cases have not been explicitly stated. First, the MUSTA scheme is applied to and tested on another equation system – a two-pressure two-fluid model. The scheme is found to be robust and accurate, but not efficient. The efficiency penalty is contrary to the hope of Toro [41] of presenting a non-costly scheme.

Next, a *direct comparison* between computations using a single-pressure and those using a two-pressure two-fluid model can be performed due to the use of the MUSTA scheme in each case. Different propositions have been set forth in the literature regarding the practical value of the pressure-relaxation approach, and the present direct comparison is thought to contribute to more certain conclusions. Here it is clearly seen that the two-pressure two-fluid model with instantaneous pressure relaxation converges to the single-pressure two-fluid model, and it should be noted that this includes any instabilities due to complex eigenvalues in the single-pressure two-fluid model. This observation is in agreement with the remarks of Karni et al. [20] and Hérard [19]. A further point to note is that the pressure relaxation is prone to cause significant numerical smearing. The present study therefore confirms the findings of

Munkejord [26] for the Roe scheme. Roe methods for two-phase flow models have been studied e.g. in [13, 20, 29, 45, 46].

Velocity relaxation will also be addressed. Instantaneous velocity relaxation in the two-fluid model produces results equal to those of the drift-flux model. Here no slip (equal gas and liquid velocity) is considered for simplicity, and it is seen that the velocity relaxation introduces much less numerical smearing than the pressure relaxation.

Section 2 briefly describes the two two-fluid models under consideration, and shows how to put them in a canonical form which makes them suitable for applying the MUSTA scheme of Section 3. Numerical simulations comparing the approaches to relaxation and testing the numerical schemes are performed in Section 4, and Section 5 concludes the paper.

2 Model formulation

This paper studies the one-dimensional two-phase flow, focusing on some mathematical key parts of the models. Such a practise is common [2, 10, 13, 31]. An attempt to include all possible two-phase flow phenomena would unnecessarily clutter the discussion. The models under study are presented in the following.

2.1 Four-equation system

Consider a model consisting of a mass-conservation equation and a momentum-balance equation for the gas (g) and liquid (ℓ) phase:

$$\frac{\partial}{\partial t}(\alpha_{\mathrm{g}}\rho_{\mathrm{g}}) + \frac{\partial}{\partial x}(\alpha_{\mathrm{g}}\rho_{\mathrm{g}}v_{\mathrm{g}}) = 0, \tag{2.1}$$

$$\frac{\partial}{\partial t}(\alpha_{\ell}\rho_{\ell}) + \frac{\partial}{\partial x}(\alpha_{\ell}\rho_{\ell}v_{\ell}) = 0, \tag{2.2}$$

$$\frac{\partial}{\partial t}(\alpha_{\mathrm{g}}\rho_{\mathrm{g}}v_{\mathrm{g}}) + \frac{\partial}{\partial x}\left(\alpha_{\mathrm{g}}\rho_{\mathrm{g}}v_{\mathrm{g}}^2\right) + \alpha_{\mathrm{g}}\frac{\partial p}{\partial x} + \Delta p_{\mathrm{i}}\frac{\partial \alpha_{\mathrm{g}}}{\partial x} = \alpha_{\mathrm{g}}\rho_{\mathrm{g}}g_x - \tau_{\mathrm{i}}, \tag{2.3}$$

$$\frac{\partial}{\partial t}(\alpha_{\ell}\rho_{\ell}v_{\ell}) + \frac{\partial}{\partial x}\left(\alpha_{\ell}\rho_{\ell}v_{\ell}^2\right) + \alpha_{\ell}\frac{\partial p}{\partial x} + \Delta p_{\mathrm{i}}\frac{\partial \alpha_{\ell}}{\partial x} = \alpha_{\ell}\rho_{\ell}g_x + \tau_{\mathrm{i}}. \tag{2.4}$$

For $k \in \{\mathrm{g}, \ell\}$, ρ_k denotes the density, v_k the velocity, α_k the volume fraction, g_x the gravitational acceleration in x direction, and p the common pressure.

$$\Delta p_{\mathrm{i}} = p - p_{\mathrm{i}}$$

is the interfacial pressure difference and τ_{i} is an interfacial momentum-exchange term to be defined in the following. By default, we will use $\tau_{\mathrm{i}} = 0$.

The volume fractions satisfy

$$\alpha_{\mathrm{g}} + \alpha_{\ell} = 1. \tag{2.5}$$

The equation of state

$$p = p_k(\rho_k) = c_k^2(\rho_k - \rho_k^\circ), \tag{2.6}$$

is employed, where the speed of sound, c_k, and the "reference density", ρ_k° are constants for each phase, constituting an assumption of constant entropy or temperature.

In the following, the Eqs. (2.1)–(2.4) with (2.5) and (2.6) will be referred to as the *four-equation system*.

2.2 Five-equation system

In Saurel and Abgrall [36], the two-fluid model was augmented with an advection equation for the volume fraction – with an added pressure-relaxation term. Here we do likewise, except that in the present case, the energy equation is disregarded for simplicity. The model then reads:

$$\frac{\partial \alpha_\mathrm{g}}{\partial t} + v_\mathrm{i}\frac{\partial \alpha_\mathrm{g}}{\partial x} = r_p(p_\mathrm{g} - p_\ell), \tag{2.7}$$

$$\frac{\partial}{\partial t}(\alpha_\mathrm{g}\rho_\mathrm{g}) + \frac{\partial}{\partial x}(\alpha_\mathrm{g}\rho_\mathrm{g}v_\mathrm{g}) = 0, \tag{2.8}$$

$$\frac{\partial}{\partial t}(\alpha_\ell\rho_\ell) + \frac{\partial}{\partial x}(\alpha_\ell\rho_\ell v_\ell) = 0, \tag{2.9}$$

$$\frac{\partial}{\partial t}(\alpha_\mathrm{g}\rho_\mathrm{g}v_\mathrm{g}) + \frac{\partial}{\partial x}\left(\alpha_\mathrm{g}\rho_\mathrm{g}v_\mathrm{g}^2\right) + \alpha_\mathrm{g}\frac{\partial p_\mathrm{g}}{\partial x} + \Delta p_\mathrm{ig}\frac{\partial \alpha_\mathrm{g}}{\partial x} = \alpha_\mathrm{g}\rho_\mathrm{g}g_x - \tau_\mathrm{i}, \tag{2.10}$$

$$\frac{\partial}{\partial t}(\alpha_\ell\rho_\ell v_\ell) + \frac{\partial}{\partial x}\left(\alpha_\ell\rho_\ell v_\ell^2\right) + \alpha_\ell\frac{\partial p_\ell}{\partial x} + \Delta p_{\mathrm{i}\ell}\frac{\partial \alpha_\ell}{\partial x} = \alpha_\ell\rho_\ell g_x + \tau_\mathrm{i}. \tag{2.11}$$

Herein, r_p is a pressure-relaxation parameter, and v_i is the average interfacial velocity, to be defined in the following. We employ the same equation of state as for the four-equation system, but here, the pressures in each phase are independent:

$$p_k = p_k(\rho_k) = c_k^2(\rho_k - \rho_k^\circ). \tag{2.12}$$

Eqs. (2.7)–(2.11) with (2.12) and (2.5) will in the following be referred to as the *five-equation system*. There are two main differences compared to the four-equation system, namely the presence of a volume-fraction advection Eq. (2.7), and independent pressures in each phase.

The coefficient matrix of the five-equation system is diagonalizable with real eigenvalues almost everywhere, except at the sonic points, see e.g., [35]. Further, simple, analytical expressions are available for the eigenvalues and eigenvectors. More details are also given in [26] for the current context. These are advantages for the five-equation system compared to the four-equation system, where analytical expressions for the eigenstructure are only available for particular choices for the constitutive relations, and for which there are regions where the hyperbolicity is lost.

2.2.1 Overview of the solution procedure

In this paper, the momentum-source term τ_i is included to act as an interfacial drag term, or velocity-relaxation term in the current jargon:

$$\tau_\mathrm{i} = r_v(v_\mathrm{g} - v_\ell), \tag{2.13}$$

where r_v is a velocity-relaxation parameter.

The relaxation terms may become large. Therefore, the equation system (2.7)–(2.11) is split in two, and solved using a fractional-step technique. The hyperbolic part of the system is (2.7)–(2.11) with

$$r_p \equiv 0, \quad \text{and} \quad r_v \equiv 0.$$

The remainder is the relaxation part:

$$\frac{\partial \alpha_\mathrm{g}}{\partial t} = r_p(p_\mathrm{g} - p_\ell), \tag{2.14}$$

$$\frac{\partial}{\partial t}(\alpha_\mathrm{g}\rho_\mathrm{g}) = 0, \tag{2.15}$$

$$\frac{\partial}{\partial t}(\alpha_\ell\rho_\ell) = 0, \tag{2.16}$$

$$\frac{\partial}{\partial t}(\alpha_\mathrm{g}\rho_\mathrm{g}v_\mathrm{g}) = r_v(v_\ell - v_\mathrm{g}), \tag{2.17}$$

$$\frac{\partial}{\partial t}(\alpha_\ell\rho_\ell v_\ell) = -r_v(v_\ell - v_\mathrm{g}). \tag{2.18}$$

Let $\boldsymbol{q}_j^n$ denote the numerical approximation to the cell average of the vector of unknowns $\boldsymbol{q}(x, t_n)$ in control volume j at time step n. With $\boldsymbol{q}_j^n$ as an initial value, the solution at the next time step, $\boldsymbol{q}_j^{n+1}$, can be found as follows:

1. Find $\boldsymbol{q}_j^*$ as the solution of the hyperbolic part of (2.7)–(2.11) at t_{n+1}.
2. Find $\boldsymbol{q}_j^n$ as the solution of the relaxation system (2.14)–(2.18) at t_{n+1} with $\boldsymbol{q}_j^*$ as initial value.

For step 1, the MUSTA scheme will be employed, and it will be detailed in Section 3. For step 2, a numerical solver for ordinary differential equations will be used for finite-rate relaxation. For infinite/ instantaneous relaxation, it is more efficient to employ the procedure detailed in the next two subsections.

2.2.2 Infinite pressure relaxation

Specific values for the pressure-relaxation parameter, r_p, are most often unknown. However, the assumption of equal phasic pressures is widespread, and can be accounted for by setting r_p to a large value. It is then more efficient to solve the problem directly than solving the system (2.14)–(2.18) of differential equations: After the hyperbolic step, the volume fraction is modified so as to render the two phasic pressures equal, keeping $\alpha_k\rho_k$ and $\alpha_k\rho_k v_k$ constant.

Munkejord [26] solved a second-degree equation for the volume fraction. In this study, however, it was found to be a more robust approach to solve a second-degree equation for the pressure instead. Such an equation is commonly solved in single-pressure two-fluid calculations, see e.g., [31]. The equation is derived by adding (2.6) multiplied by α_g, to (2.6) multiplied by α_ℓ, and using (2.5), and its positive solution is

$$p = \frac{-\psi_2 + \sqrt{\psi_2^2 - 4\psi_1\psi_3}}{2\psi_1}, \tag{2.19}$$

where

$$\psi_1 = 1, \tag{2.20}$$

$$\psi_2 = c_g^2\left(\rho_g^\circ - \alpha_g\rho_g\right) + c_\ell^2\left(\rho_\ell^\circ - \alpha_\ell\rho_\ell\right), \tag{2.21}$$

$$\psi_3 = c_g^2 c_\ell^2\left(\rho_g^\circ\rho_\ell^\circ - \alpha_g\rho_g\rho_\ell^\circ - \alpha_\ell\rho_\ell\rho_g^\circ\right). \tag{2.22}$$

The remaining variables are then found in a straightforward manner, using the equation of state.

Note that the present procedure is somewhat simpler than the one discussed in [36], since in the present case, the energy equation is not considered.

It should be emphasized that for instantaneous pressure relaxation, the volume-fraction advection Eq. (2.7) becomes singular, and the two phasic pressures become equal. Hence it is expected that the equation system reduces to the four-equation system.

2.2.3 Velocity relaxation

The instantaneous velocity-relaxation procedure can be applied after the hyperbolic step, or after the instantaneous pressure-relaxation step, if applicable. Here we only consider no slip ($v_g = v_\ell$), and we employ the procedure derived by Saurel and Abgrall [36], simplified to the case of no energy equation. The procedure simply consists of changing $\alpha_g\rho_g v_g$ and $\alpha_\ell\rho_\ell v_\ell$ so that $v_g = v_\ell$, while keeping $\sum_k(\alpha_k\rho_k v_k)$, $\alpha_g\rho_g$, $\alpha_\ell\rho_\ell$ and α_g constant. The relaxed (mixture) velocity is

$$v = v_g = v_\ell = \frac{\alpha_g\rho_g v_{g,0} + \alpha_\ell\rho_\ell v_{\ell,0}}{\alpha_g\rho_g + \alpha_\ell\rho_\ell}, \tag{2.23}$$

where the subscript 0 denotes the initial value supplied to the velocity-relaxation procedure. This is the mass-weighted velocity.

For computations with the five-equation system presented in this article, instantaneous pressure relaxation and no velocity relaxation will be employed, unless otherwise stated.

If instantaneous velocity relaxation is employed in the four-equation system, or in the five-equation system with instantaneous pressure relaxation, it is expected that a drift-flux model is recovered [16]. The drift-flux model considered here consists

of a continuity equation for each phase, and a momentum-balance equation for the mixture momentum, that is, the sum of (2.3) and (2.4). In addition, a constitutive relation for the relative velocity between the phases (the slip) is needed. A MUSTA scheme for the drift-flux model was discussed by Munkejord et al. [27].

2.2.4 Interface velocity

Following Saurel and Abgrall [36], we will also use the mass-weighted velocity as a model for the average interfacial velocity in (2.7):

$$v_\mathrm{i} = \frac{\alpha_\mathrm{g}\rho_\mathrm{g}v_\mathrm{g} + \alpha_\ell\rho_\ell v_\ell}{\alpha_\mathrm{g}\rho_\mathrm{g} + \alpha_\ell\rho_\ell}. \tag{2.24}$$

2.3 Interfacial-pressure model

Both in the four-equation and the five-equation system, a model is needed for the interfacial pressure difference. In this work, the model of Bestion [4] is employed:

$$p_k - p_{\mathrm{i}k} = \Delta p_{\mathrm{i}k} = \delta\frac{\alpha_\mathrm{g}\alpha_\ell\rho_\mathrm{g}\rho_\ell}{\alpha_\mathrm{g}\rho_\ell + \alpha_\ell\rho_\mathrm{g}}(v_\mathrm{g} - v_\ell)^2. \tag{2.25}$$

The main justification of the expression is to render the four-equation system hyperbolic for a reasonable range of parameters [4, 37]. Following Evje and Flåtten [13], we take $\delta = 1.2$, unless otherwise stated.

2.4 Canonical form of the equation systems

Both two-fluid models of the preceding subsections can be written in the following form:

$$\frac{\partial \boldsymbol{q}}{\partial t} + \frac{\partial \boldsymbol{f}(\boldsymbol{q})}{\partial x} + \boldsymbol{B}(\boldsymbol{q})\frac{\partial \boldsymbol{w}(\boldsymbol{q})}{\partial x} = \boldsymbol{s}(\boldsymbol{q}). \tag{2.26}$$

2.4.1 Four-equation system

For the model of Section 2.1, we obtain

$$\boldsymbol{q} = \begin{bmatrix} \alpha_\mathrm{g}\rho_\mathrm{g} \\ \alpha_\ell\rho_\ell \\ \alpha_\mathrm{g}\rho_\mathrm{g}v_\mathrm{g} \\ \alpha_\ell\rho_\ell v_\ell \end{bmatrix}, \quad \boldsymbol{f}(\boldsymbol{q}) = \begin{bmatrix} \alpha_\mathrm{g}\rho_\mathrm{g}v_\mathrm{g} \\ \alpha_\ell\rho_\ell v_\ell \\ \alpha_\mathrm{g}\rho_\mathrm{g}v_\mathrm{g}^2 + \alpha_\mathrm{g}\Delta p_\mathrm{i} \\ \alpha_\ell\rho_\ell v_\ell^2 + \alpha_\ell\Delta p_\mathrm{i} \end{bmatrix}, \quad \boldsymbol{s}(\boldsymbol{q}) = \begin{bmatrix} 0 \\ 0 \\ \alpha_\mathrm{g}\rho_\mathrm{g}g_x - \tau_\mathrm{i} \\ \alpha_\ell\rho_\ell g_x + \tau_\mathrm{i} \end{bmatrix}, \tag{2.27}$$

$$\boldsymbol{B}(\boldsymbol{q}) = \begin{bmatrix} 0 \\ 0 \\ \alpha_\mathrm{g} \\ \alpha_\ell \end{bmatrix}, \qquad \boldsymbol{w}(\boldsymbol{q}) = p - \Delta p_\mathrm{i}. \tag{2.28}$$

2.4.2 Five-equation system

The model of Section 2.2 can be expressed with

$$\boldsymbol{q} = \begin{bmatrix} \alpha_\mathrm{g} \\ \alpha_\mathrm{g}\rho_\mathrm{g} \\ \alpha_\ell\rho_\ell \\ \alpha_\mathrm{g}\rho_\mathrm{g}v_\mathrm{g} \\ \alpha_\ell\rho_\ell v_\ell \end{bmatrix}, \quad \boldsymbol{f}(\boldsymbol{q}) = \begin{bmatrix} 0 \\ \alpha_\mathrm{g}\rho_\mathrm{g}v_\mathrm{g} \\ \alpha_\ell\rho_\ell v_\ell \\ \alpha_\mathrm{g}\rho_\mathrm{g}v_\mathrm{g}^2 + \alpha_\mathrm{g}\Delta p_\mathrm{i} \\ \alpha_\ell\rho_\ell v_\ell^2 + \alpha_\ell\Delta p_\mathrm{i} \end{bmatrix}, \quad \boldsymbol{s}(\boldsymbol{q}) = \begin{bmatrix} r_p(p_\mathrm{g} - p_\ell) \\ 0 \\ 0 \\ \alpha_\mathrm{g}\rho_\mathrm{g}g_x - \tau_\mathrm{i} \\ \alpha_\ell\rho_\ell g_x + \tau_\mathrm{i} \end{bmatrix}, \tag{2.29}$$

$$\boldsymbol{B}(\boldsymbol{q}) = \begin{bmatrix} v_\mathrm{i} & 0 & 0 & 0 & 0 \\ 0 & 0 & 0 & 0 & 0 \\ 0 & 0 & 0 & 0 & 0 \\ 0 & 0 & 0 & \alpha_\mathrm{g} & 0 \\ 0 & 0 & 0 & 0 & \alpha_\ell \end{bmatrix}, \qquad \boldsymbol{w}(\boldsymbol{q}) = \begin{bmatrix} \alpha_\mathrm{g} \\ 0 \\ 0 \\ p_\mathrm{g} - \Delta p_\mathrm{ig} \\ p_\ell - \Delta p_{\mathrm{i}\ell} \end{bmatrix}. \tag{2.30}$$

3 The MUSTA scheme

A MUSTA scheme was derived for the four-equation system in Munkejord et al. [28] by using the framework of formally path-consistent schemes of Parés [32]. In this work, that scheme is applied to the five-equation system. With the canonical form of the equation system given in Section 2.4.2, the scheme can be applied rather directly.

The derivations in [28] will not be repeated here, but the MUSTA building blocks and algorithm will be recalled for convenience.

3.1 Building blocks

Consider the equation system

$$\frac{\partial \boldsymbol{q}}{\partial t} + \frac{\partial \boldsymbol{f}(\boldsymbol{q})}{\partial x} + \boldsymbol{B}(\boldsymbol{q})\frac{\partial \boldsymbol{w}(\boldsymbol{q})}{\partial x} = \boldsymbol{0}. \tag{3.1}$$

It can be discretized as

$$\frac{1}{\Delta t}(\boldsymbol{q}_j^{n+1} - \boldsymbol{q}_j^n) + \frac{1}{\Delta x}\Big((\boldsymbol{f}_{j+\frac{1}{2}} - \boldsymbol{f}_{j-\frac{1}{2}}) + (\boldsymbol{d}^+_{j-\frac{1}{2}} + \boldsymbol{d}^-_{j+\frac{1}{2}})\Big) = \boldsymbol{0}, \tag{3.2}$$

with

$$\boldsymbol{d}^+_{j+\frac{1}{2}} = \boldsymbol{B}_{j+\frac{1}{2}}\big(\boldsymbol{w}_{j+1} - \boldsymbol{w}_{j+\frac{1}{2}}\big), \tag{3.3}$$

$$\boldsymbol{d}^-_{j+\frac{1}{2}} = \boldsymbol{B}_{j+\frac{1}{2}}\big(\boldsymbol{w}_{j+\frac{1}{2}} - \boldsymbol{w}_j\big). \tag{3.4}$$

Herein, expressions are needed for $\boldsymbol{f}_{j+\frac{1}{2}}$, $\boldsymbol{w}_{j+\frac{1}{2}}$ and $\boldsymbol{B}_{j+\frac{1}{2}}$, as will be detailed in the following.

3.1.1 The FORCE scheme

The basic building block of MUSTA is the first-order centred (FORCE) scheme of Toro [40] see also [8, 43]. It has the least numerical dissipation of the first-order central schemes that are stable for all CFL numbers less than unity [8].

The FORCE numerical flux is defined as the arithmetic mean of the Lax–Friedrichs flux and the Richtmyer Lax–Wendroff flux:

$$\boldsymbol{f}^{FORCE}_{j+\frac{1}{2}} = \frac{1}{2}\Big(\boldsymbol{f}^{LF}_{j+\frac{1}{2}} + \boldsymbol{f}^{LW}_{j+\frac{1}{2}}\Big). \tag{3.5}$$

It is then natural to assume the same averaging for the cell-interface value of the non-conservative variables vector, $\boldsymbol{w}_{j+1/2}$:

$$\boldsymbol{w}^{FORCE}_{j+\frac{1}{2}} = \frac{1}{2}\Big(\boldsymbol{w}^{LF}_{j+\frac{1}{2}} + \boldsymbol{w}^{LW}_{j+\frac{1}{2}}\Big). \tag{3.6}$$

3.1.2 The Lax–Friedrichs scheme

For the non-conservative system (3.1), De Vuyst [11] proposed the Lax–Friedrichs discretization

$$\boldsymbol{f}^{LF}_{j+\frac{1}{2}} = \frac{1}{2}\Big(\boldsymbol{f}(\boldsymbol{q}_j) + \boldsymbol{f}(\boldsymbol{q}_{j+1})\Big) + \frac{1}{2}\frac{\Delta x}{\Delta t}(\boldsymbol{q}_j - \boldsymbol{q}_{j+1}), \tag{3.7}$$

with

$$\boldsymbol{d}^{\pm}_{j+\frac{1}{2}} = \frac{1}{2}\boldsymbol{B}_{j+\frac{1}{2}}(\boldsymbol{w}_{j+1} - \boldsymbol{w}_j), \tag{3.8}$$

that is

$$\boldsymbol{w}^{LF}_{j+\frac{1}{2}} = \frac{1}{2}(\boldsymbol{w}_j + \boldsymbol{w}_{j+1}). \tag{3.9}$$

3.1.3 The Richtmyer scheme

It is the two-step Richtmyer version of the Lax–Wendroff scheme that is employed in the FORCE scheme. First, the cell-interface solution is evolved one half time step using a simple Lax–Friedrichs scheme:

$$\begin{aligned}\boldsymbol{q}^{n+\frac{1}{2}}_{j+\frac{1}{2}} = \frac{1}{2}\Big(\boldsymbol{q}^{n}_{j} + \boldsymbol{q}^{n+\frac{1}{2}}_{j+1}\Big) - \frac{1}{2}\frac{\Delta t}{\Delta x}\Big(\boldsymbol{f}(\boldsymbol{q}^{n}_{j+1}) - \boldsymbol{f}(\boldsymbol{q}^{n}_{j})\Big) \\ - \frac{1}{2}\frac{\Delta t}{\Delta x}\boldsymbol{B}^{n}_{j+\frac{1}{2}}(\boldsymbol{w}^{n}_{j+1} - \boldsymbol{w}^{n}_{j}).\end{aligned} \tag{3.10}$$

Then the numerical cell-interface values to be plugged into (3.5) and (3.6) are given as:

$$\boldsymbol{f}^{LW}_{j+\frac{1}{2}} = \boldsymbol{f}(\boldsymbol{q}^{n+\frac{1}{2}}_{j+\frac{1}{2}}), \tag{3.11}$$

$$\boldsymbol{w}^{LW}_{j+\frac{1}{2}} = \boldsymbol{w}(\boldsymbol{q}^{n+\frac{1}{2}}_{j+\frac{1}{2}}). \tag{3.12}$$

3.1.4 The cell-interface matrix

As shown in [28], a formally path-consistent scheme can be achieved by calculating the cell-interface matrix, $\boldsymbol{B}_{j+1/2}$, from an appropriate average state between the cells j and $j+1$. Here, that can be done by simply choosing

$$\boldsymbol{B}_{j+\frac{1}{2}} = \begin{bmatrix} 0 \\ 0 \\ \alpha_{\mathrm{g},j+\frac{1}{2}} \\ \alpha_{\ell,j+\frac{1}{2}} \end{bmatrix}, \tag{3.13}$$

for the four-equation system, and

$$\boldsymbol{B}(\boldsymbol{q}) = \begin{bmatrix} v_{\mathrm{i},j+\frac{1}{2}} & 0 & 0 & 0 & 0 \\ 0 & 0 & 0 & 0 & 0 \\ 0 & 0 & 0 & 0 & 0 \\ 0 & 0 & 0 & \alpha_{\mathrm{g},j+\frac{1}{2}} & 0 \\ 0 & 0 & 0 & 0 & \alpha_{\ell,j+\frac{1}{2}} \end{bmatrix}, \tag{3.14}$$

for the five-equation system. Herein, $\alpha_{\mathrm{g},j+1/2}$ and $v_{\mathrm{i},j+1/2}$ are calculated by arithmetic averaging, and $\alpha_{\ell,j+1/2} = 1 - \alpha_{\mathrm{g},j+1/2}$, as always.

We are now equipped to delve into the MUSTA algorithm.

3.2 Algorithm

In the multi-stage (MUSTA) approach [39,44], the numerical flux, $\boldsymbol{f}_{j+1/2}$, at the cell interface is found by employing a two-step procedure: First, a numerical approximation to the solution of the cell-interface Riemann problem produces two modified states at either side of the interface. These states are then fed into a numerical flux function to obtain the sought flux, $\boldsymbol{f}_{j+1/2}$. There are several conceivable choices for the numerical flux function. Titarev and Toro [39] employed the FORCE flux, whereas Toro and Titarev [44] promoted a development termed the GFORCE flux. We prefer the "classical" FORCE flux, which is slightly simpler and seems to be more robust.

The MUSTA procedure employed here is similar to the previous ones for the Euler equations [39,44] and for the drift-flux model [27], but it is extended to account for the non-conservative terms in the governing equations. The present exposition is from [28].

For calculating the numerical flux, $\boldsymbol{f}_{j+1/2}$, and the non-conservative variables vector, $\boldsymbol{w}_{j+1/2}$, the Riemann problem at the cell interface, $x_{j+1/2}$, is transformed to a local grid:

$$\frac{\partial \boldsymbol{q}}{\partial t} + \frac{\partial \boldsymbol{f}(\boldsymbol{q})}{\partial \xi} + \boldsymbol{B}(\boldsymbol{q}) \frac{\partial \boldsymbol{w}(\boldsymbol{q})}{\partial \xi} = \boldsymbol{0}, \tag{3.15a}$$

$$\boldsymbol{q}(\xi, 0) = \begin{cases} \boldsymbol{q}_j = \boldsymbol{q}_L, & \text{if } \xi < 0, \\ \boldsymbol{q}_{j+1} = \boldsymbol{q}_R, & \text{if } \xi \geq 0, \end{cases} \tag{3.15b}$$

where the position $\xi = 0$ corresponds to $x_{j+1/2}$. This local Riemann problem is then solved approximately by employing the FORCE scheme, where the local grid is indexed by n, and, following Titarev and Toro [39], we set $\Delta\xi \equiv \Delta x$:

$$\frac{1}{\Delta t_{loc}}(\boldsymbol{q}_n^{m+1} - \boldsymbol{q}_n^m) + \frac{1}{\Delta x}(\boldsymbol{f}_{n+\frac{1}{2}}^{FORCE} - \boldsymbol{f}_{n-\frac{1}{2}}^{FORCE}) + \frac{1}{\Delta x}\Big(\boldsymbol{B}_{n-\frac{1}{2}}(\boldsymbol{w}_n - \boldsymbol{w}_{n-\frac{1}{2}}^{FORCE}) + \boldsymbol{B}_{n+\frac{1}{2}}(\boldsymbol{w}_{n+\frac{1}{2}}^{FORCE} - \boldsymbol{w}_n)\Big) = \boldsymbol{0}. \tag{3.16}$$

Herein, $\boldsymbol{f}_{n+1/2}^{FORCE}$, $\boldsymbol{w}_{n+1/2}^{FORCE}$ and

$$\boldsymbol{B}_{n+\frac{1}{2}} = \boldsymbol{B}_{n+\frac{1}{2}}(\boldsymbol{q}_n, \boldsymbol{q}_{n+1})$$

are calculated as described in the preceding subsections, while

$$\boldsymbol{w}_n = \boldsymbol{w}(\boldsymbol{q}_n).$$

Terms without a time index are evaluated at stage m. The local pseudo-time step, Δt_{loc}, is calculated using the Courant–Friedrichs–Lewy (CFL) criterion on the local grid:

$$\Delta t_{loc} = \frac{C_{loc}\Delta x}{\max\limits_{1\le n\le 2N}\Big(\max\limits_{1\le p\le d}|\lambda_n^p|\Big)}, \tag{3.17}$$

where d is the dimension of the system (2.26), and the local CFL number, C_{loc}, is a parameter in the method. In this work we follow [39] and set $C_{loc} = 0.9$ for all the computations. For the four-equation system, the maximum eigenvalues, λ, are approximated using the estimates of [13].

The initial conditions and the numbering of the local grid are illustrated in Fig. 1.

The M-stage MUSTA algorithm for the flux $\boldsymbol{f}$ and the vector $\boldsymbol{w}$ can be summarized as follows:

1. For each local cell $n = 1, \ldots, 2N$, compute the flux $\boldsymbol{f}^{FORCE,m}_{n+1/2}$ from (3.5), the vector $\boldsymbol{w}^{FORCE,m}_{n+1/2}$ from (3.6) and the coefficient matrix $\boldsymbol{B}^m_{n+1/2}$ from (3.13) or (3.14) using data from stage m.
2. If $m = M$, then return $\boldsymbol{f}^{FORCE,M}_{N+1/2}$ and $\boldsymbol{w}^{FORCE,M}_{N+1/2}$, else continue.
3. Update the local solution using (3.16) for $n = 1, \ldots, 2N$.
4. Apply extrapolation boundary conditions; $\boldsymbol{q}_0^m = \boldsymbol{q}_1^m$, and $\boldsymbol{q}_{2N+1}^m = \boldsymbol{q}_{2N}^m$. Augment m and repeat from 1.

Thus, when the MUSTA scheme is used to solve (3.2)–(3.4), $\boldsymbol{f}_{j+1/2}$ and $\boldsymbol{w}_{j+1/2}$ are found using the above algorithm, whereas $\boldsymbol{B}_{j+1/2}$ and the other quantities are calculated using data from the global grid, as usual. As shown in [28], the above procedure reduces to the standard conservative MUSTA algorithm [39, 44] when $\boldsymbol{B}$ is constant in time and space.

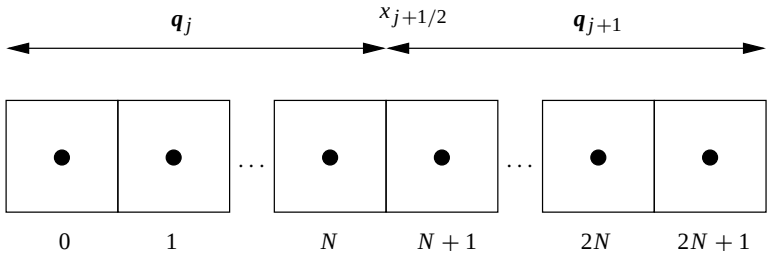

Figure 1: Initial values and cell numbering for the local MUSTA grid.

It should be noted that to avoid spurious oscillations, it is necessary to choose $M \leq 2N$ in the MUSTA algorithm [27]. In the following, we will denote the M-stage MUSTA scheme with $2N$ local cells by MUSTA_{M-2N}. Further, we refer to the MUSTA scheme for the four-equation system as MUSTA4 (see Section 2.4.1), and to that of the five-equation system as MUSTA5 (see Section 2.4.2).

It is possible to save some computational time by refining the above MUSTA algorithm. In fact, since we are solving a Riemann problem, and since we are only interested in the solution at the mid cell interface, it is not necessary to include all the local cells $n = 1, \ldots, 2N$ in all the local time steps, as noted by Titarev and Toro [39, 44]. For instance, in the first local time step, only the two mid cells enter into the calculation. In the next step, one cell has to be added at each side, as the waves propagate at most one cell per time step. When the waves have reached the boundary of the local grid, one cell can be excluded at each side, etc. This "diamond optimization" was suggested by Toro and Titarev [44] and has been used for all the computations presented here.

3.3 Second-order extension

To obtain second-order spatial accuracy for smooth solutions, a semi-discrete version of the monotone upwind-centred scheme for conservation laws (MUSCL) [30, 50] has been employed. Herein, a piecewise linear function is constructed by using the data $\{\boldsymbol{q}_j(t)\}$. At each side of the interface, $x_{j+1/2}$, we have values from the linear approximations in the neighbouring cells. These are denoted by

$$\boldsymbol{q}_j^R = \boldsymbol{q}_j + \frac{\Delta x}{2}\boldsymbol{\sigma}_j, \tag{3.18}$$

$$\boldsymbol{q}_{j+1}^L = \boldsymbol{q}_{j+1} - \frac{\Delta x}{2}\boldsymbol{\sigma}_{j+1}, \tag{3.19}$$

where $\boldsymbol{\sigma}_j$ are the slopes calculated using a suitable slope-limiter function. Some are listed in [23, Section 9.2]. The *minmod* slope is

$$\sigma_j = \text{minmod}\left(\frac{q_j - q_{j-1}}{\Delta x}, \frac{q_{j+1} - q_j}{\Delta x}\right), \tag{3.20}$$

where the minmod function is defined by

$$\operatorname{minmod}(a,b) = \begin{cases} 0, & \text{if } ab \leq 0, \\ a, & \text{if } |a| < |b| \text{ and } ab > 0, \\ b, & \text{if } |a| \geq |b| \text{ and } ab > 0. \end{cases} \tag{3.21}$$

The *monotonized central-difference (MC)* slope [49] is

$$\sigma_j = \operatorname{minmod}\left(\left(\frac{q_{j+1}-q_{j-1}}{2\Delta x}\right), 2\left(\frac{q_j - q_{j-1}}{\Delta x}\right), 2\left(\frac{q_{j+1}-q_j}{\Delta x}\right)\right). \tag{3.22}$$

We also have the van Leer [48] [see 49] limiter

$$\sigma_j = \begin{cases} \dfrac{2(q_j - q_{j-1})(q_{j+1}-q_j)}{(q_j - q_{j-1}) + (q_{j+1}-q_j)}, & \text{if } \operatorname{sgn}(q_j - q_{j-1}) = \operatorname{sgn}(q_{j+1}-q_j), \\ 0, & \text{otherwise.} \end{cases} \tag{3.23}$$

The slope limiting is applied component-wise to the variable-vector. There are several possible choices of variables to use. Here, the choice has been made to employ $[\alpha_g, p, v_g, v_\ell]$ for the four-equation system and $[\alpha_g, \rho_g, v_g, \rho_\ell, v_\ell]$ for the five-equation system. After this procedure, the flux $\boldsymbol{f}_{j+1/2}$ and the vector $\boldsymbol{w}_{j+1/2}$ can be computed from $(\boldsymbol{q}_j^R, \boldsymbol{q}_{j+1}^L)$, precisely as described in the preceding subsections. That is, it is only the Riemann problem (3.15) to be solved on the local grid that is modified according to (3.18). It should be noted that the cell-interface matrix is still a function of the non-reconstructed variables. That is, $(\boldsymbol{q}_j^R, \boldsymbol{q}_{j+1}^L)$ are not involved in the evaluation of $\boldsymbol{B}_{j+1/2}$.

For use with the MUSCL scheme, the system of balance Eq. (2.26) is semi-discretized:

$$\frac{d\boldsymbol{q}_j}{dt} + \frac{\boldsymbol{f}_{j+\frac{1}{2}} - \boldsymbol{f}_{j-\frac{1}{2}}}{\Delta x} + \frac{\boldsymbol{d}^+_{j-\frac{1}{2}} + \boldsymbol{d}^-_{j+\frac{1}{2}}}{\Delta x} = \boldsymbol{s}_j. \tag{3.24}$$

To obtain a second-order solution in time, the two-stage second-order strong-stability-preserving (SSP) Runge–Kutta (RK) method is employed (see for instance [21]). With (3.24) of the form

$$\frac{d\boldsymbol{q}_j}{dt} = \mathscr{L}(\boldsymbol{q}_j), \tag{3.25}$$

the two-stage second-order SSP-RK scheme can be written as

$$\boldsymbol{q}_j^{(1)} = \boldsymbol{q}^n + \Delta t \mathscr{L}(\boldsymbol{q}^n), \tag{3.26a}$$

$$\boldsymbol{q}^{n+1} = \frac{1}{2}\boldsymbol{q}^n + \frac{1}{2}\boldsymbol{q}^{(1)} + \frac{1}{2}\Delta t \mathscr{L}(\boldsymbol{q}^{(1)}). \tag{3.26b}$$

Herein, $\boldsymbol{q}_j^n$ is the vector of unknowns from time step n, $\boldsymbol{q}_j^{n+1}$ is the sought values at the next time step, while $\boldsymbol{q}_j^{(1)}$ represents intermediate values.

In conjunction with the first-order MUSTA scheme, the time stepping is performed using the Forward Euler method.

Table 1: Parameters employed in the equation of state.

	c_k (m/s)	ρ_k° (kg/m^3)
gas (g)	$\sqrt{10^3}$	0
liquid (ℓ)	1000	999.9

4 Numerical simulations

In this section, the MUSTA4 and MUSTA5 schemes will be analysed by performing numerical benchmark tests from the literature. In particular, effects of pressure and velocity relaxation will be discussed.

Independent numerical schemes will be employed for reference. For the four-equation system, the Roe4 scheme presented by Evje and Flåtten [13] and further discussed by Munkejord [26] will be used. The reference for the five-equation system is the Roe5 scheme by Munkejord [26]. The Roe scheme for the drift-flux model, Roe3, of Flåtten and Munkejord [15] will also be used for benchmarking.

All the presented calculations have been performed employing the equation-of-state parameters given in Table 1.

4.1 Moving discontinuity

It is essential that numerical schemes "disturb" the flow as little as possible. In particular, for a uniform pressure and velocity flow, the pressure and velocities should remain uniform, even if there is a jump in the volume fraction [1].

This basic test was done by performing a calculation in a 12 m long horizontal tube, where the initial state consists of uniform velocities and pressures, see Table 2. A similar case was considered in [7]. At the middle of the tube, the gas volume fraction jumps from $1-\varepsilon$ to ε, where $\varepsilon = 1 \times 10^{-6}$. This gives practically single-phase flow on each side of the discontinuity, even though pure phases are not explicitly accounted for in the present framework. Due to the numerical calculations for the equation of state, ε cannot go too close to zero. A similar limitation was also reported in [36].

Calculations were performed for both the four-equation and the five-equation system. For the former, the MUSCL-MUSTA4$_{4-4}$ scheme (four local steps and four local cells) was employed with the van Leer slope slope (3.23). For the latter, the MUSCL-MUSTA5$_{4-4}$ scheme is somewhat less robust, and was employed with the minmod slope (3.20). All the calculations were run using a CFL number of $C = 0.5$ on a 200-cell grid. The gas volume fraction at time $t = 0.03$ s is displayed in Fig. 2. Ideally, the volume fraction should be advected, but not smeared. As shown in the figure, some smearing takes place, and more so for MUSTA5 than for MUSTA4. In both cases, the results are oscillation-free.

No disturbances are introduced in the other variables to plotting accuracy. However, it is interesting to evaluate the disturbances quantitatively. Let us define the

Table 2: Initial state for the moving-discontinuity problem.

Quantity	Symbol (unit)	Left	Right
Gas volume fraction	α_g (–)	$1-\varepsilon$	ε
Pressure	p (MPa)	0.1	0.1
Gas velocity	v_g (m/s)	100	100
Liquid velocity	v_ℓ (m/s)	100	100

maximum relative pressure disturbance for the calculation as

$$\mathscr{E}_p = \frac{1}{p^0} \max_{\forall n} \left\{ | \max_{\forall j} p_j^n - \min_{\forall j} p_j^n | \right\}, \tag{4.1}$$

where p^0 is the initial pressure, j is the spatial index and superscript n denotes the time step. In this case $\mathscr{E}_p \approx 7 \times 10^{-9}$ for MUSTA4, while $\mathscr{E}_p \approx 1 \times 10^{-8}$ for MUSTA5. These are thought to be satisfactory values.

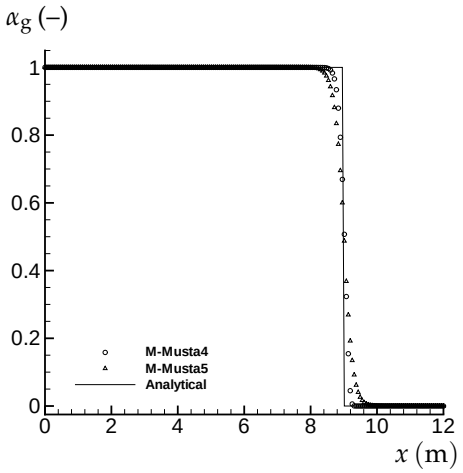

Figure 2: Gas volume fraction for the moving discontinuity. MUSCL-MUSTA$_{4-4}$, 200 cells, $C = 0.5$.

4.2 Water faucet

The water-faucet test case is one of the most common benchmark cases for numerical methods for one-dimensional two-fluid models. It was introduced by Ransom [34] and has been studied for instance in [9, 13, 16, 26, 31, 47]. In particular, this test reveals the ability of the method to capture mass transport. The calculated pressure profiles are sensitive to the boundary conditions, but the velocities and the volume fraction are not [25].

The initial flow field is uniform, and the values are given in Table 3. The inlet boundary conditions are equal to the initial values for the gas volume fraction and for

Table 3: Initial state in the water-faucet test problem.

Quantity	Symbol (unit)	Value
Gas $vol.\,frac.$	α_g (–)	0.2
Pressure	p (MPa)	0.1
Gas velocity	v_g (m/s)	0.0
Liquid velocity	v_ℓ (m/s)	10.0

the gas and liquid velocities. A pressure equal to the initial pressure is specified at the outlet. At time $t = 0$, gravity ($g = 9.81\,\mathrm{m/s^2}$) is turned on, and the liquid column starts thinning as a discontinuity moves towards the exit. In the following, the results are given at $t = 0.6$s. An approximate analytical solution can be found for instance in [13]. Even though there is a difference between the solution of the two-fluid model obtained on very fine grids and this approximate solution, it is customarily used as a reference in the volume-fraction plots.

Let us first consider the effect of the number of local time steps (M) and local cells ($2N$) in the MUSTA solver. As noted by Munkejord et al. [27], M and $2N$ cannot be varied independently. We need to take $M \leq 2N$ to avoid oscillations due to boundary effects in the MUSTA procedure. Fig. 3 shows volume-fraction profiles obtained on a 100-cell grid for a CFL number of $C = 0.9$ without using MUSCL reconstruction, that is, for the first-order schemes. In Fig. 3(a), the results for the MUSTA4 scheme for the four-equation system are shown. The volume-fraction profile calculated using the first-order Roe4 scheme for the same conditions has been plotted for reference. As can be seen, for an increasing number of local cells and time steps, the volume-fraction profiles of the MUSTA4 scheme become sharper. However, as many as 200 local steps are needed for the MUSTA4 scheme to produce a volume-fraction profile

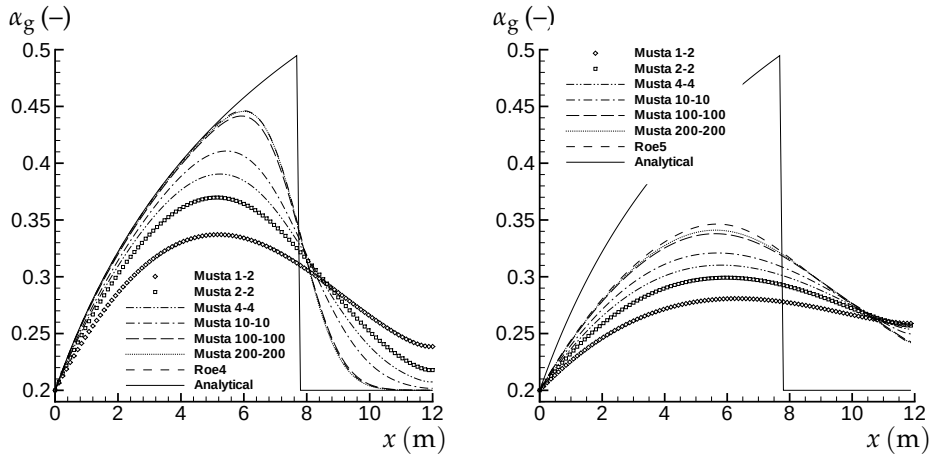

(a) MUSTA4 (b) MUSTA5

Figure 3: Gas volume fraction for the water faucet. Effect of increasing number of stages and local cells in the MUSTA4 and MUSTA5 schemes. 100 cells, $C = 0.9$.

comparable to that of the Roe4 scheme. The many local steps lead to a substantial CPU-time consumption.

An analogous comparison for the MUSTA5 scheme for the five-equation system is given in Fig. 3(b). Two main differences with respect to the MUSTA4 scheme can be observed. First, the MUSTA5 scheme is significantly more diffusive than the MUSTA4 scheme. This is due to the pressure relaxation, as will be further illustrated in the following. Second, even with 200 local steps, the MUSTA5 procedure is more diffusive than the corresponding Roe5 procedure.

The faucet case has also been calculated with the more accurate MUSCL schemes. Herein, various slope-limiter functions have been tested, namely the superbee (see [23], Section 9.2) and the minmod slope (3.20), the van Leer slope slope (3.23) and the monotonized central-difference (MC) slope (3.22). The latter three slopes gave acceptable results, whereas the superbee slope gave oscillations. The MC slope gave the best results in this case.

Volume-fraction profiles for MUSCL-MUSTA$_{4-4}$ ($M = 4$ local time steps and $2N = 4$ local cells in the MUSTA procedure) are given in Fig. 4. The profiles in Fig. 4(a) obtained using the MUSCL-MUSTA4 scheme are sharp and non-oscillatory, albeit not quite as good as the results presented in [26] for the Roe4 scheme with characteristic flux limiting.

Fig. 4(b) shows volume-fraction profiles calculated using the MUSCL-MUSTA5 scheme. They are also non-oscillatory, but they are much more smeared than the ones of MUSCL-MUSTA4. Indeed, by comparing for instance the 100-cell solution in Fig. 4(b) with the one for MUSTA4$_{4-4}$ in Fig. 3(a), one can see that the MUSCL version of the MUSTA5 method gives less resolution than the first-order MUSTA4 scheme.

Pressure profiles for the faucet case are given in Fig. 5. Here, no analytical solution

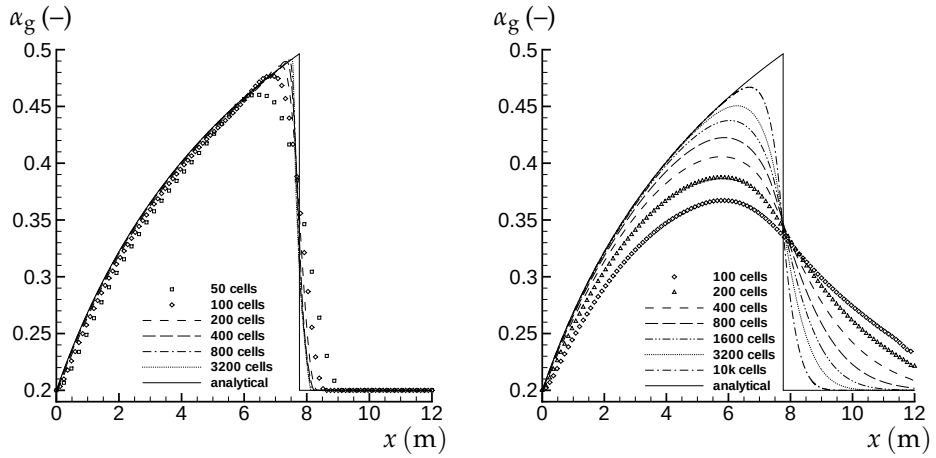

(a) MUSCL-MUSTA4 (b) MUSCL-MUSTA5

Figure 4: Gas volume fraction for the water faucet. Convergence of the MUSCL-MUSTA4$_{4-4}$ and -MUSTA5$_{4-4}$ schemes using the MC slope. $C = 0.5$.

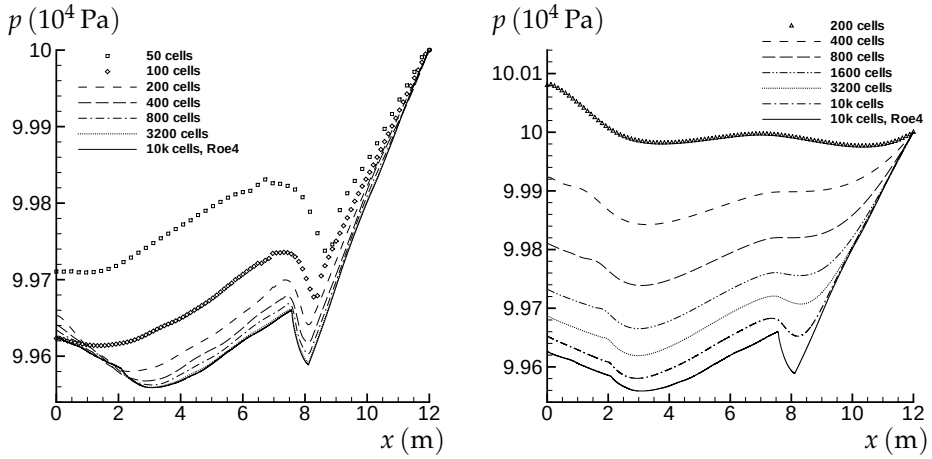

(a) MUSCL-MUSTA4 (b) MUSCL-MUSTA5

Figure 5: Pressure for the water faucet. Convergence of the MUSCL-MUSTA4_{4-4} and -MUSTA5_{4-4} schemes using the MC slope. $C = 0.5$.

is available, so a calculation with the MC-limited Roe4 scheme on a fine grid (10 000 cells) has been plotted as reference. In Fig. 5(a), the solution of MUSCL-MUSTA4 on a 3200-cell grid is quite close to the reference solution. In Fig. 5(b), the MUSCL-MUSTA5 solution still is a bit off, even for 10 000 cells. In general, MUSTA5 needs a much finer grid than MUSTA4 to capture the pressure profile inherent in the solution of the faucet problem.

The effect of reducing the time-step length on a fixed grid of 200 cells is studied in Figs. 6–7. Herein, $M = 2$ and $N = 8$ has been used in the MUSTA procedure to obtain

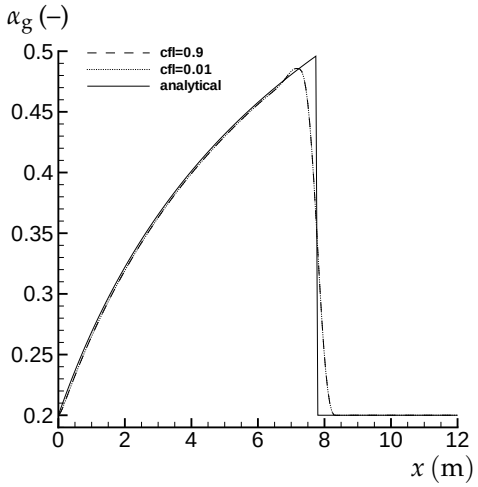

Figure 6: Gas volume fraction for the water faucet. Effect of time-step length on the MUSCL-MUSTA4_{8-8} scheme using the MC slope. 200 cells.

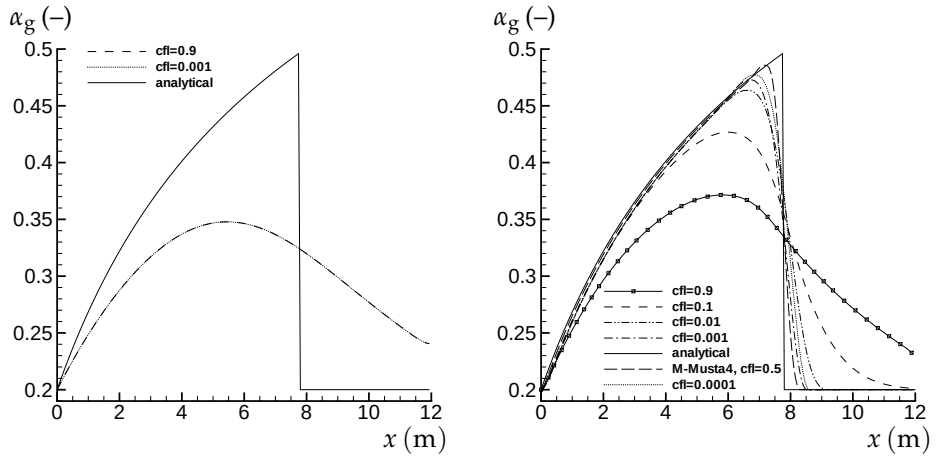

(a) No limiter (first order) (b) MC slope

Figure 7: Gas volume fraction for the water faucet. Effect of time-step length on the (MUSCL-) MUSTA5$_{8-8}$ scheme with and without using the MC slope. 200 cells.

a somewhat higher resolution. For the MUSTA4 and the MUSCL-MUSTA4 schemes, time-step refinement gives only a miniscule effect. The solutions for $C = 0.9$ and for $C = 0.001$ are the same to plotting accuracy. This is shown in Fig. 6 for the MUSCL-MUSTA4 scheme.

The MUSTA5 method is a bit peculiar. For the first-order MUSTA5 scheme, the results shown in Fig. 7(a) are smeared, but non-varying as the CFL number is reduced. For the MUSCL-MUSTA5 scheme, on the other hand, a large improvement in the resolution is achieved for small CFL numbers, see Fig. 7(b). A similar effect

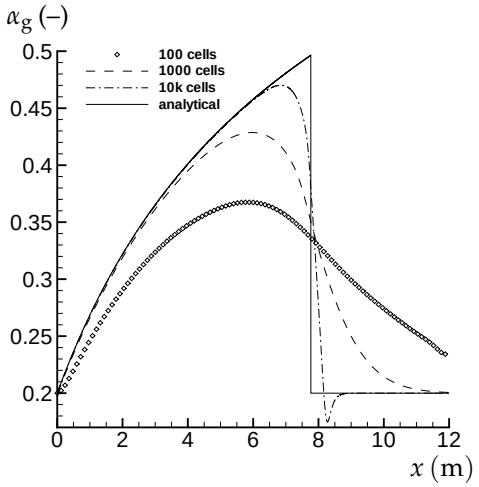

Figure 8: Gas volume fraction for the water faucet. Grid refinement for the MUSCL-MUSTA5$_{4-4}$, method employing $\delta = 0$ in (2.25), the MC slope and $C = 0.5$.

was observed in [26] for the Roe5 scheme. It goes without saying, however, that keeping the CFL number in the order of 1×10^{-4} is not particularly efficient. Further, as Fig. 7(b) shows, MUSCL-MUSTA5 never quite attains the reference profile calculated using the MUSCL-MUSTA4 scheme using a CFL number of $C = 0.5$.

One of the perceived advantages of performing calculations using the five-equation system with instantaneous pressure relaxation instead of keeping the four-equation system, is that the former equation system is hyperbolic everywhere, except at the sonic points. The justification of the Eq. (2.25) for the interfacial pressure difference is to render the four-equation system hyperbolic in a reasonable range, rather than physical considerations. Fig. 8 shows the volume-fraction profiles from calculations having been performed with the MUSCL-MUSTA5_{4-4} method on various grids and with a constant CFL number of $C = 0.5$. In these calculations, the parameter δ was set equal to zero in (2.25). In this case, the four-equation system is non-hyperbolic with complex eigenvalues, while the five-equation system is not. Even so, the figure clearly shows that at fine grids, an instability develops. This kind of instability is normally associated with a non-hyperbolic model [37]. Further grid refinements leads to a breakdown of the simulation.

A similar observation was made by Karni et al. [20] employing a Roe-type method with pressure relaxation for a two-fluid model including an energy equation.

4.3 Toumi's shock tube

This shock-tube problem was introduced by Toumi [45] and it has been studied e.g., in [14, 26, 31, 38]. A tube of length 100 m is divided by a membrane in the middle. At $t = 0$, the membrane ruptures, and the flow starts evolving. The initial conditions are displayed in Table 4. For this problem, $\delta = 2$ has been employed in the Eq. (2.25), as was also done in [14, 31]. No source terms were considered, except for relaxation terms, where noted.

4.3.1 Instantaneous pressure relaxation

Fig. 9 shows the physical variables calculated at $t = 0.08$ s. The MUSCL-MUSTA5 method with the van Leer slope has been employed, using a CFL number of $C = 0.5$. A reference solution has been calculated using the Roe4 scheme on a fine grid of 10 000 cells. For Toumi's shock tube, the Roe scheme needs an entropy fix to converge to a physically plausible solution. Here, the fix of Harten [18] [see also e.g., 23, Section 5.3.5] was employed.

Table 4: Initial state in Toumi's shock tube.

Quantity	Symbol (unit)	Left	Right
Gas $vol.\,frac.$	α_g (–)	0.25	0.10
Pressure	p (MPa)	20	10
Gas velocity	v_g (m/s)	0	0
Liquid velocity	v_ℓ (m/s)	0	0

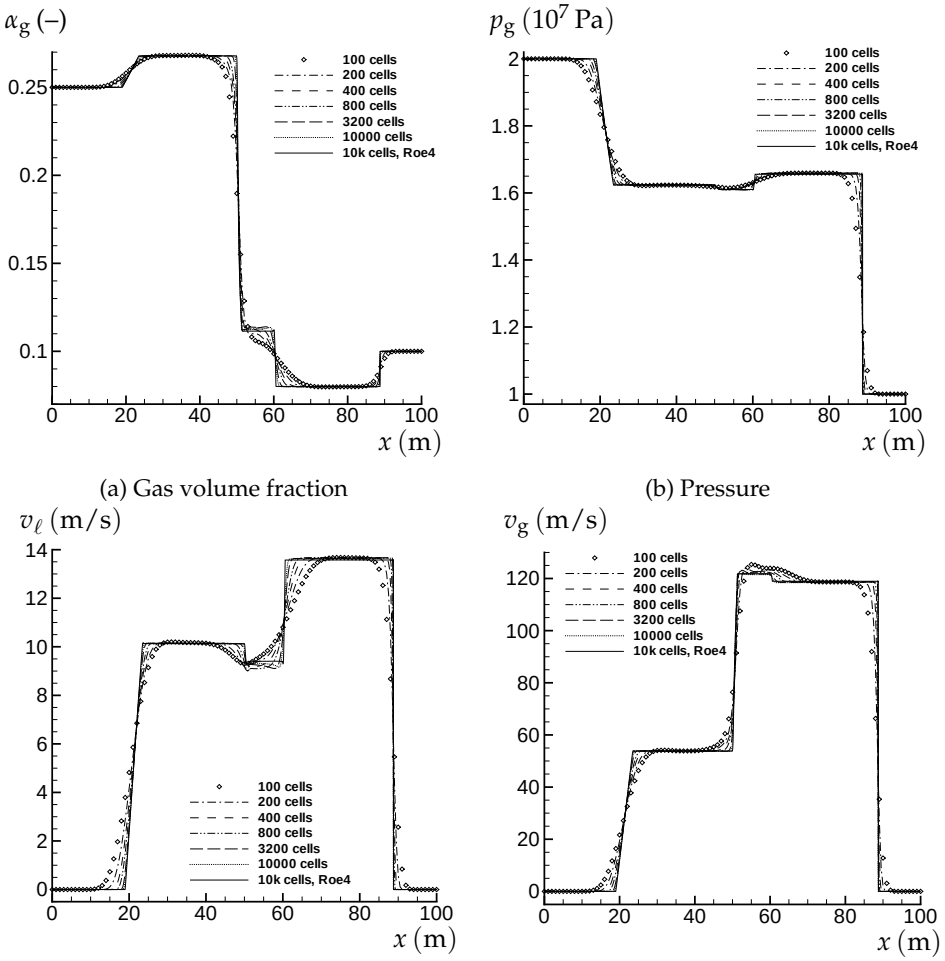

(a) Gas volume fraction

(b) Pressure

(c) Liquid velocity

(d) Gas velocity

Figure 9: Toumi's shock tube at $t = 0.08\,\mathrm{s}$. Convergence of the MUSCL-MUSTA5 method using the van Leer slope. $C = 0.5$.

As can be seen from the plots, the results of the MUSCL-MUSTA5 method converge towards those of the Roe4 scheme. This also indicates that the five-equation system with instantaneous pressure relaxation converges to the four-equation system. The figures further show that the MUSCL-MUSTA5 method converges quite slowly in the middle of the tube, where volume-fraction waves are present.

4.3.2 Finite pressure relaxation

In the computations presented so far, instantaneous pressure relaxation was always used in the MUSTA5 method. We will now study the effect of finite pressure relaxation in the five-equation system. That is, the pressure-relaxation parameter, r_p, will attain finite values, while the velocity-relaxation parameter still is $r_v = 0$.

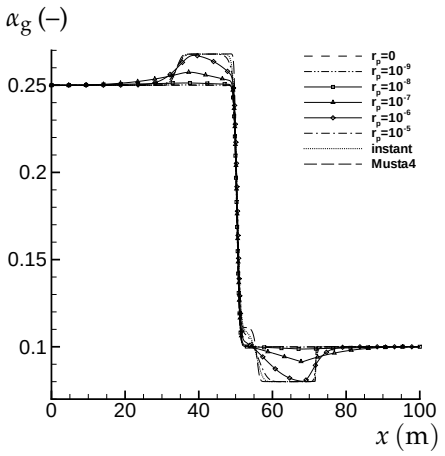

(a) Gas volume fraction

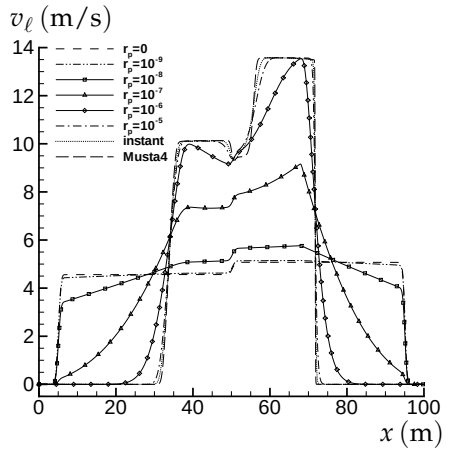

(b) Liquid velocity

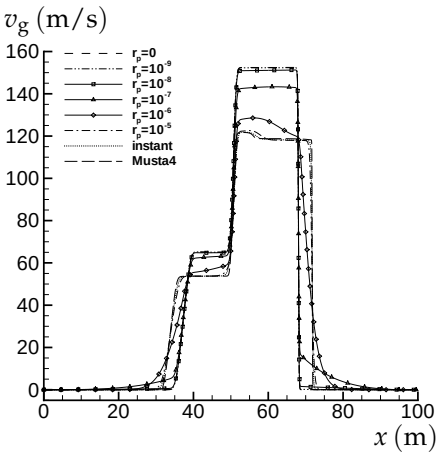

(c) Gas velocity

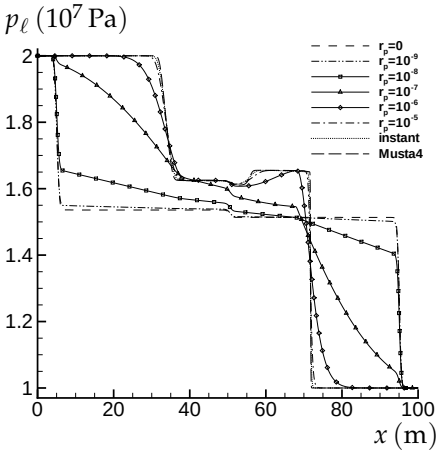

(d) Liquid pressure

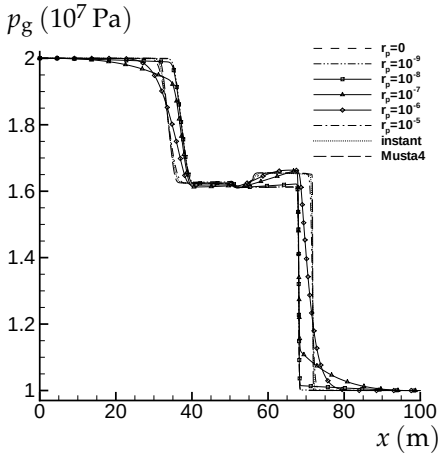

(e) Gas pressure

Figure 10: Toumi's shock tube at $t = 0.045$s. Effect of the pressure-relaxation parameter r_p in the MUSTA5 (first-order) method on a 2000-cell grid. $C = 0.9$.

Toumi's shock tube has been calculated with varying values of the pressure-relaxation parameter, r_p. The results are displayed in Fig. 10. Here, the first-order MUSTA5 method has been used with a 2000-cell grid and a CFL number of $C = 0.9$. The calculations have been stopped at $t = 0.045\,\mathrm{s}$ to avoid interaction between the waves and the domain boundaries. Data obtained with the MUSTA4 scheme are plotted for reference.

Fig. 10(b) shows a plot of the liquid velocity. For a low value of the pressure-relaxation parameter, r_p, the two sonic waves have reached about $x = 5\mathrm{m}$ and $x = 95\mathrm{m}$. As r_p is increased, those two fast sonic waves are gradually suppressed, and the effect of the gas phase becomes more and more apparent.

The approximate speed of the sonic waves can be read from the figure. For a low r_p, the average speed of the right-going wave is $45\mathrm{m}/0.045\mathrm{s} = 1000\mathrm{m/s}$, which closely corresponds to the liquid speed of sound. When the pressure-relaxation parameter is increased, the "resultant" sonic speed is reduced to that of the four-equation model, as is evident from the fact that the profiles approach those calculated with the MUSTA4 scheme.

For the gas velocity shown in Fig. 10(c), it can be seen that the sonic speed approaches that of the four-equation system from below. The sonic waves travel with the gas speed of sound for low values of r_p, increasing to the sonic speed of the two-fluid model for instantaneous pressure relaxation.

The liquid and gas pressures are displayed in Figs. 10(d) and 10(e), and it can be observed how the two independent pressures converge to one as the relaxation parameter r_p is increased.

Figs. 10(b) and 10(c) (or 10(d) and 10(e)) reveal that the five-equation system without pressure relaxation has five waves; two sonic waves for the liquid, two sonic waves for the gas, and one mass wave (volume-fraction wave). For instantaneous pressure relaxation, we observe two sonic waves and two mass waves, as for the four-equation system.

The performance of the MUSTA4 scheme and the MUSTA5 method with instantaneous pressure relaxation can be compared by studying the long-dashed and the dotted line for instance in Fig. 10(b). It can be seen that MUSTA5 generally smeares the solution more than MUSTA4, and that the difference is largest at the middle of the tube, that is, for the volume-fraction waves. It is hypothesized that the reason for the increased smearing of the volume-fraction waves lies in the coupling between the pressure and the volume fraction in the volume-fraction advection Eq. (2.7); the pressure being associated with fast-travelling waves.

4.3.3 Finite velocity relaxation

We now turn to the effect of finite velocity relaxation. It will be studied by adding velocity-relaxation terms to the momentum equations of the four-equation system, but it could equally well have been done by considering the five-equation system with infinite pressure relaxation.

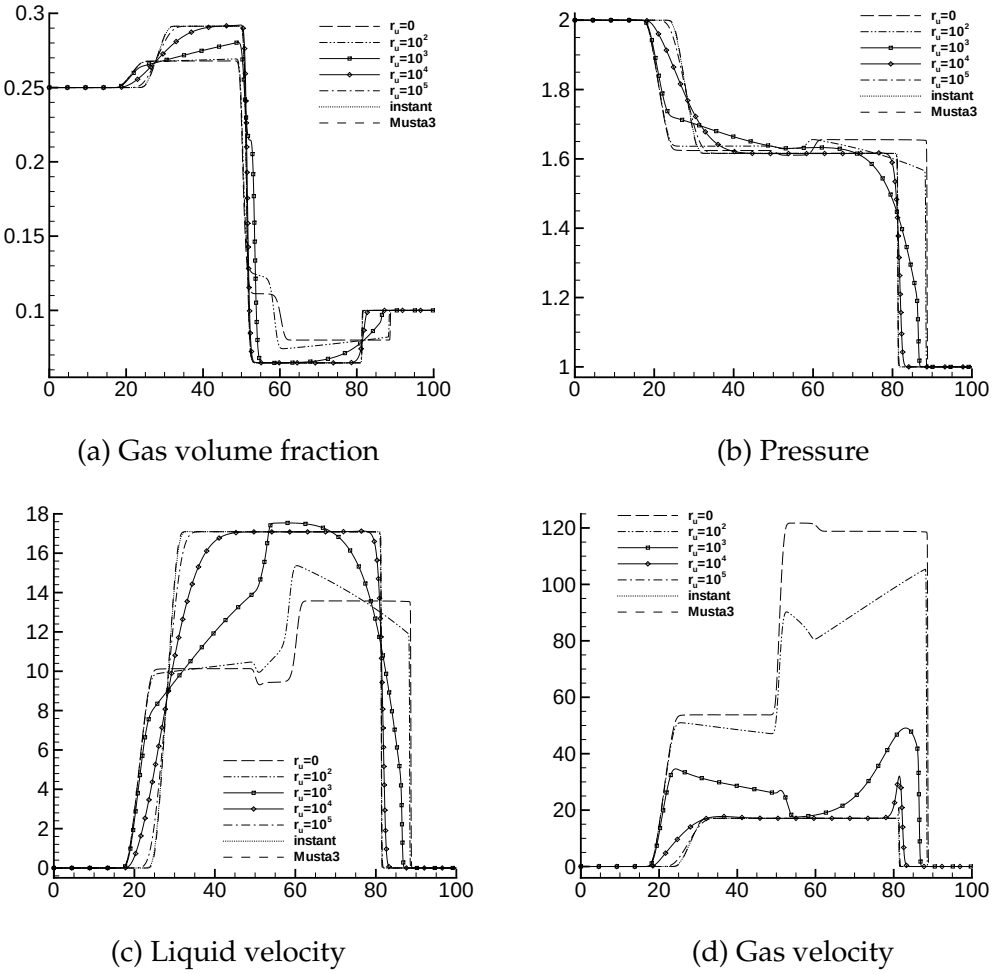

(a) Gas volume fraction

(b) Pressure

(c) Liquid velocity

(d) Gas velocity

Figure 11: Toumi's shock tube at $t = 0.08$ s. Effect of the velocity-relaxation parameter r_v in the MUSTA4 (first-order) method on a 2000-cell grid. $C = 0.9$.

The four-equation system with infinite velocity relaxation corresponds to the drift-flux model. Therefore, the MUSTA scheme for the drift-flux model studied in [27] will be used as a reference scheme. It will be referred to as MUSTA3. Here, we only consider no slip, that is,

$$v_{\mathrm{g}} = v_{\ell}.$$

The effect of increasing the velocity-relaxation parameter, r_v, in the MUSTA4 scheme, can be studied in Fig. 11. As for the case of finite pressure relaxation, the first-order version of the scheme has been employed on a 2000-cell grid with a CFL number of $C = 0.9$. The results are plotted at $t = 0.08$ s, like in Fig. 9.

Consider Fig. 11(a) for the gas volume fraction. The curve for no velocity relaxation, $r_v = 0$, is similar to the ones in Fig. 9(a). As the velocity-relaxation parameter

is increased, the two volume-fraction waves at the middle of the tube are gradually merged into one. At the same time, the two sonic waves are modified, so that the resultant waves for the instant-relaxation case are slower. It is well known that the drift-flux model has a lower sonic speed than the two-fluid model for a wide range of parameters.

Further, as shown in Figs. 11(c) and 11(d), the liquid and gas velocities gradually approach each other as the velocity-relaxation parameter is increased.

It is interesting to note that in Fig. 11, the curve for MUSTA4 with instantaneous velocity relaxation (dotted line) practically lies on top of the one for MUSTA3 (dashed line). See for instance Fig. 11(a). This is in contrast to the case for pressure relaxation, where the relaxation procedure introduces a considerable amount of smearing.

The plots in Fig. 11 show that the transistion between no velocity relaxation and instant velocity relaxation is smooth, as was also the case for the pressure relaxation in Fig. 10. However, an attempt to physically interpret the intermediate plots will not be made here.

4.3.4 Computational cost

A comparison of the CPU-time consumption of various MUSTA$_{M-2N}$ schemes and their corresponding Roe reference schemes is given in Table 5. The calculations were run using a CFL number of $C = 0.5$. The data are calculated on a 1600-cell grid. Other grids were also tried, but no grid dependency was detected. The columns labelled "1. order" show the CPU time of the first-order MUSTA$_{M-2N}$ scheme divided by that of the first-order Roe scheme. The columns marked "limited" show the same relation for the MUSCL-MUSTA$_{M-2N}$ scheme using the van Leer slope limiter and the Roe scheme using the van Leer flux limiter.

As the number of local time steps, M, and local cells, $2N$, are increased in the MUSTA schemes, their computational cost strongly grows. The number of local time steps and cells needed to roughly match the Roe scheme in accuracy is case dependent. For the shock-tube case considered in [27] for the drift-flux model, four local steps and cells was considered acceptable. As noted in Section 4.2, about 100 local steps and cells are needed for the water-faucet case for the two-fluid model. It can be observed that the CPU-time relation is roughly equal for MUSTA3/ Roe3 and MUSTA4/ Roe4, while that of MUSTA5/ Roe5 is much higher. This is because the Roe3 scheme for the

Table 5: Toumi's shock tube. Comparison of CPU-time consumption between MUSTA$_{M-2N}$ and Roe schemes.

	Drift-flux		4-eq. syst.		5-eq. syst.	
M-2N	1. order	limited	1. order	limited	1. order	limited
2-2	0.26	0.58	0.25	0.62	2.62	6.38
4-4	0.58	1.23	0.54	1.19	5.28	11.4
6-6	0.99	2.04	0.93	1.94	8.99	18.3
8-8	1.49	3.03	1.42	2.93	13.6	27.2

drift-flux model and the Roe4 scheme for the two-fluid model need a numerical diagonalization of the coefficient matrix. Roe5, on the other hand, has analytical expressions for the eigenvalues and eigenvector matrix.

The table shows that the second-order Roe schemes are relatively cheaper than the MUSCL-MUSTA schemes. The reason for this is that in the Roe scheme, most of the work required to assemble the high-resolution terms has already been performed during the diagonalization of the coefficient matrix. In MUSCL-MUSTA, on the other hand, the piecewise reconstruction of the data comes fully in addition to the calculations done in the basic scheme.

The above results show that the MUSTA schemes do not in general fulfill the intention of Toro [41] of being non-CPU-costly. Since the MUSTA schemes are relatively CPU-intensive when a high degree of accuracy is desired, they will be advantageous mainly for equation systems where a Roe matrix is not available, or where the Roe scheme is not robust enough. One example of the latter case is the water-air separation case discussed by Munkejord et al. [28].

5 Conclusions

The multi-stage centred (MUSTA) scheme of Munkejord et al. [28] for non-conservative two-fluid models has been applied to the two-fluid model augmented with a volume-fraction advection equation (five-equation system). It has been analysed numerically and compared to the MUSTA scheme for the "isentropic" two-fluid model (four-equation system). The use of analogous numerical schemes allowed for an evaluation of the approach of augmenting the two-fluid model with a volume-fraction advection equation and employing instantaneous pressure relaxation.

A main motivation for employing the augmented two-fluid model is its analytical eigenstructure, easing the construction of approximate Riemann solvers. However, the most common application of this approach is to use it for the simulation of two-phase flow problems where the pressures of the phases are so strongly coupled that instantaneous pressure relaxation is required.

The numerical simulations presented here demonstrate that the five-equation system converges to the four-equation system when the pressure relaxation approaches infinity. Indeed, in cases such as for zero interfacial pressure difference, the relaxation terms in the five-equation system induce the kind of instabilities which are associated with complex eigenvalues in the four-equation system, even if the five-equation system has real eigenvalues.

Therefore, the approach of employing an augmented two-fluid model with instantaneous pressure relaxation should be regarded as a *numerical method* to solve the single-pressure two-fluid model. Moreover, calculations have shown that this approach introduces a large amount of numerical smearing, particularly for the slow-moving volume-fraction (mass-transport) waves. The reason for this is probably the extra coupling between the fast-moving sonic waves and the volume-fraction waves

introduced by the volume-fraction advection equation with its relaxation term.

Velocity relaxation in the four-equation system has also been tested. As expected, the four-equation system with instantaneous velocity relaxation produces identical results to those of the drift-flux model. The velocity relaxation did not introduce any noticeable numerical smearing.

The MUSTA schemes produced accurate and non-oscillatory results both for the four-equation and the five-equation system. However, in cases where volume-fraction waves are important, it may be necessary to take many local steps in the MUSTA procedure to reduce the smearing of these waves. This limits the computational efficiency.

Acknowledgments

This work was financed by SINTEF Energy Research and the Research Council of Norway. Thanks are due to Tore Flåtten at SINTEF Energy Research for the fruitful discussions. Knut Erik Teigen at the Norwegian University of Science and Technology (NTNU) has read and commented the manuscript.

References

[1] R. ABGRALL, *How to prevent pressure oscillations in multicomponent flow calculations: A quasi conservative approach*, J .Comput. Phys., 125 (1996), pp. 150–160.

[2] R. ABGRALL AND R. SAUREL, *Discrete equations for physical and numerical compressible multiphase mixtures*, J. Comput. Phys., 186 (2003), pp. 361–396.

[3] M. R. BAER AND J. W. NUNZIATO, *A two-phase mixture theory for the deflagration-to-detonation transition (DDT) in reactive granular materials*, Int. J. Multiphase Flow., 12 (1986), pp. 861–889.

[4] D. BESTION, *The physical closure laws in the CATHARE code*, Nucl. Eng. Design., 124 (1990), pp. 229–245.

[5] C. E. CASTRO AND E. F. TORO, *A Riemann solver and upwind methods for a two-phase flow model in non-conservative form*, Int. J. Numer. Meth. Fl., 50 (2006), pp. 275–307.

[6] M. J. CASTRO, P. G. LEFLOCH, M. L. MUÑOS, AND C. PARÉS, *Why many theories of shock waves are necessary: Convergence error in formally path-consistent schemes*, J. Comput. Phys., 227 (2008), pp. 8107–8129.

[7] C. H. CHANG AND M. S. LIOU, *A robust and accurate approach to computing compressible multiphase flow: Stratified flow model and AUSM$^+$-up scheme*, J. Comput. Phys., 225 (2007), pp. 840–873.

[8] G. Q. CHEN AND E. F. TORO, *Centered difference schemes for nonlinear hyperbolic equations*, J. Hyperbolic Differ. Equ., 1 (2004), pp. 531–566.

[9] F. COQUEL, K. EL AMINE, E. GODLEWSKI, B. PERTHAME, AND P. RASCLE, *A numerical method using upwind schemes for the resolution of two-phase flows*, J. Comput. Phys., 136 (1997), pp. 272–288.

[10] J. CORTES, A. DEBUSSCHE, AND I. TOUMI, *A density perturbation method to study the eigenstructure of two-phase flow equation systems*, J. Comput. Phys., 147 (1998), pp. 463–484.

[11] F. DE VUYST, *Stable and accurate finite volume method based on pure convexity arguments for hyperbolic systems of conservation law*, J. Comput. Phys., 193 (2004), pp. 426–468.

[12] D. A. DREW AND S. L. PASSMAN, Theory of Multicomponent Fluids, volume 135 of Applied Mathematical Sciences, Springer-Verlag, New York (1999), ISBN 0-387-98380-5.
[13] S. EVJE AND T. FLÅTTEN, *Hybrid flux-splitting schemes for a common two-fluid model*, J. Comput. Phys., 192 (2003), pp. 175–210.
[14] S. EVJE AND T. FLÅTTEN, *Hybrid central-upwind schemes for numerical resolution of two-phase flows*, ESAIM – Math. Model. Num., 39 (2005), pp. 253–273.
[15] T. FLÅTTEN AND S. T. MUNKEJORD, *The approximate Riemann solver of Roe applied to a drift-flux two-phase flow model*, ESAIM – Math. Model. Num., 40 (2006), pp. 738–764.
[16] H. GUILLARD AND F. DUVAL, *A Darcy law for the drift velocity in a two-phase flow model*, J. Comput. Phys., 224 (2007), pp. 288–313.
[17] W. D. GUO, J. S. LAI, AND G. F. LIN, *Finite-volume multi-stage schemes for shallow-water flow simulations*, Int. J. Numer. Meth. Fl., 57 (2008), pp. 177–204.
[18] A. HARTEN, *High resolution schemes for hyperbolic conservation laws*, J. Comput. Phys., 49 (1983), pp. 357–393.
[19] J. M. HÉRARD AND O. HURISSE, *A simple method to compute standard two-fluid models*, Int. J. Comput. Fluid D., 19 (2005), pp. 475–482.
[20] S. KARNI, E. KIRR, A. KURGANOV, AND G. PETROVA, *Compressible two-phase flows by central and upwind schemes*, ESAIM – Math. Model. Num., 38 (2004), pp. 477–493.
[21] D. I. KETCHESON AND A. C. ROBINSON, *On the practical importance of the SSP property for Runge-Kutta time integrators for some common Godunov-type schemes*, Int. J. Numer. Meth. Fl., 48 (2005), pp. 271–303.
[22] M. H. LALLEMAND, A. CHINNAYYA, AND O. LE METAYER, *Pressure relaxation procedures for multiphase compressible flows*, Int. J. Numer. Meth. Fl., 49 (2005), pp. 1–56.
[23] R. J. LEVEQUE, Finite Volume Methods for Hyperbolic Problems, Cambridge University Press, Cambridge, UK (2002), ISBN 0-521-00924-3.
[24] P. LOILIER, C. OMBGA-ESSAMA, AND C. THOMPSON, *Numerical experiments of two-phase flow in pipelines with a two-fluid compressible model*, in: Proceedings, 12th International Conference on Multiphase Production Technology '05, BHR Group Ltd, Barcelona, Spain (2005).
[25] S. T. MUNKEJORD, *Partially-reflecting boundary conditions for transient two-phase flow*, Commun. Numer. Meth. En., 22 (2006), pp. 781–795.
[26] S. T. MUNKEJORD, *Comparison of Roe-type methods for solving the two-fluid model with and without pressure relaxation*, Comput. Fluids., 36 (2007), pp. 1061–1080.
[27] S. T. MUNKEJORD, S. EVJE, AND T. FLÅTTEN, *The multi-stage centred-scheme approach applied to a drift-flux two-phase flow model*, Int. J. Numer. Meth. Fl., 52 (2006), pp. 679–705.
[28] S. T. MUNKEJORD, S. EVJE, AND T. FLÅTTEN, *A MUSTA scheme for a nonconservative two-fluid model*, SIAM. J. Sci. Comput., 31 (2009), pp. 2587–2622.
[29] M. NDJINGA, A. KUMBARO, F. DE VUYST, AND P. LAURENT-GENGOUX, *Numerical simulation of hyperbolic two-phase flow models using a Roe solver*, Nucl. Eng. Des., 238 (2008), pp. 2075–2083, ICONE-14 – 14th International Conference on Nuclear Energy.
[30] S. OSHER, *Convergence of generalized MUSCL schemes*, SIAM. J. Numer. Anal., 22 (1985), pp. 947–961.
[31] H. PAILLÈRE, C. CORRE, AND J. R. GARCA CASCALES, *On the extension of the AUSM+ scheme to compressible two-fluid models*, Comput. Fluids., 32 (2003), pp. 891–916.
[32] C. PAILLÈRE, *Numerical methods for nonconservative hyperbolic systems: A theoretical framework*, SIAM. J. Numer. Anal., 44 (2006), pp. 300–321.
[33] J. D. RAMSHAW AND J. A. TRAPP, *Characteristics, stability, and short-wavelength phenomena in two-phase flow equation systems*, Nucl. Sci. Eng., 66 (1978), pp. 93–102.

[34] V. H. RANSOM, Faucet Flow, in: Numerical Benchmark Tests, volume 3 of Multiphase Science and Technology, G. F. HEWITT, J. M. DELHAYE, AND N. ZUBER, editors, pp. 465–467, Hemisphere/ Springer, Washington, USA (1987), ISBN 0-89116-561-4.

[35] V. H. RANSOM AND D. L. HICKS, *Hyperbolic two-pressure models for two-phase flow*, J. Comput. Phys., 53 (1984), pp. 124–151.

[36] R. SAUREL AND R. ABGRALL, *A multiphase Godunov method for compressible multifluid and multiphase flow*, J. Comput. Phys., 150 (1999), pp. 425–467.

[37] J. H. STUHMILLER, *The influence of interfacial pressure forces on the character of two-phase flow model equations*, Int. J. Multiphase Flow., 3 (1977), pp. 551–560.

[38] I. TISELJ AND S. PETELIN, *Modelling of two-phase flow with second-order accurate scheme*, J. Comput. Phys., 136 (1997), pp. 503–521.

[39] V. A. TITAREV AND E. F. TORO, *MUSTA schemes for multi-dimensional hyperbolic systems: analysis and improvements*, Int. J. Numer. Meth. Fl., 49 (2005), pp. 117–147.

[40] E. F. TORO, Riemann Solvers and Numerical Methods for Fluid Dynamics, 2nd edition, Springer-Verlag, Berlin (1999), ISBN 3-540-65966-8.

[41] E. F. TORO, Multi-Stage Predictor-Corrector Fluxes for Hyperbolic Equations, in: Isaac Newton Institute for Mathematical Sciences Preprint Series, University of Cambridge, UK (2003), NI03037-NPA, available from `http://www.newton.cam.ac.uk/preprints200-3.html`.

[42] E. F. TORO, *MUSTA: A multi-stage numerical flux*, Appl. Numer. Math., 56 (2006), pp. 1464–1479.

[43] E. F. TORO AND S. J. BILLETT, *Centred TVD schemes for hyperbolic conservation laws*, IMA. J. Numer. Anal., 20 (2000), pp. 47–79.

[44] E. F. TORO AND V. A. TITAREV, *MUSTA fluxes for systems of conservation laws*, J. Comput. Phys., 216 (2006), pp. 403–429.

[45] I. TOUMI, *An upwind numerical method for two-fluid two-phase flow models*, Nucl. Sci. Eng., 123 (1996), pp. 147–168.

[46] I. TOUMI AND A. KUMBARO, *An approximate linearized Riemann solver for a two-fluid model*, J. Comput. Phys., 124 (1996), pp. 286–300.

[47] J. A. TRAPP AND R. A. RIEMKE, *A nearly-implicit hydrodynamic numerical scheme for two-phase flows*, J. Comput. Phys., 66 (1986), pp. 62–82.

[48] B. VAN LEER, *Towards the ultimate conservative difference scheme II. Monotonicity and conservation combined in a second-order scheme*, J. Comput. Phys., 14 (1974), pp. 361–370.

[49] B. VAN LEER, *Towards the ultimate conservative difference scheme IV. A new approach to numerical convection*, J. Comput. Phys., 23 (1977), pp. 276–299.

[50] B. VAN LEER, *Towards the ultimate conservative difference scheme V. A second-order sequel to Godunov's method*, J. Comput. Phys., 32 (1979), pp. 101–136.